


國立交通大學

物理研究所

碩士論文

天體微中子與宇宙線起源之微中子流量比較

The comparison of neutrino flux from astrophysical sources
and that from GZK interactions.



研究生：謝念潔

指導教授：林貴林 教授

中華民國九十九年七月

天體微中子與宇宙線起源之微中子流量比較

The comparison of neutrino flux from astrophysical sources
and that from GZK interactions.

研 究 生： 謝念潔

Student: Nien-Chieh Hsieh

指 導 教 授： 林貴林

Advisor: Guey-Lin Lin

國立交通大學
物 理 研 究 所
碩 士 論 文



A Thesis
Submitted to Institute of Physics
National Chiao Tung University
in Partial Fulfillment of the Requirements
for the Degree of
Master
in
Physics
July, 2010
Hsinchu City, Taiwan, Republic of China

中華民國九十九年七月

天體微中子與宇宙線起源之微中子流量比較

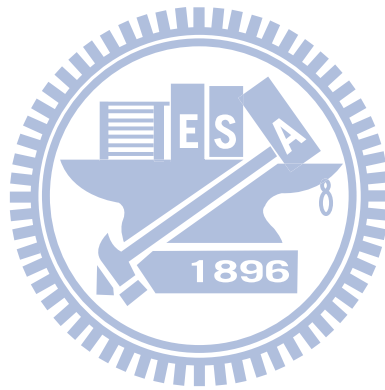
學生： 謝念潔

指導教授： 林貴林

國立交通大學物理研究所

摘 要

非常高能量的微中子是由天體和宇宙線起源而來。不同的微中子來源會導致不同的微中子味比例。本論文中，我們在不同能量範圍下比較GRB微中子流量和GZK微中子流量，藉由計算這兩個來源積分而來的流量比例，作為選擇微中子閾值能量的方法。我們提出一個統計方法，由微中子望遠鏡的味量測去重建微中子流量的比例。



The comparison of neutrino flux from astrophysical sources and that from GZK interactions.

Student: Nien-Chieh Hsieh

Advisor: Guey-Lin Lin

Submitted to Institute of Physics
National Chiao Tung University

ABSTRACT

Very high energy neutrinos come from astrophysical sources and GZK interactions. Different neutrino sources produce different neutrino flavor ratios. In this thesis, we compare GRB neutrino flux with GZK neutrino flux in different energy ranges. The ratio between integrated neutrinos fluxes from these two sources are calculated as a function of chosen neutrino threshold energy. We propose a statistical method to reconstruct such a ratio from flavor measurements of neutrino telescopes.



致 謝

感謝林貴林老師這兩年來的指導，總是非常有耐心的指引我研究上的問題，也感謝黃明輝老師、王正祥老師平時給予的建議和教導。感謝學長姊和同學們一直以來給予的幫忙，特別要感謝宗哲學長幫助我解決程式上遇到的困難，光昶學長給我論文寫作的建議，還有貝禎學姐平日的熱情與照顧，因為有你們才能讓我的研究生生活順利劃下句點。

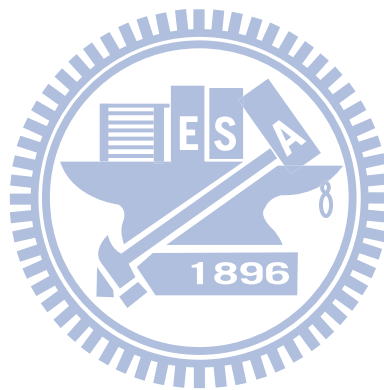
感謝我的父母親，在我遇到挫折時給我最大的支持與鼓勵，讓我繼續努力向前走。感謝我的好朋友們，一路上的分享與陪伴，使我的研究生生活不孤單。最後感謝所有幫助過我的人，謝謝你們。



Contents

中文摘要	i
Abstract	ii
致謝	iii
1 Introduction	1
2 High Energy Neutrino Sources and Neutrino Flavor Ratio	3
2.1 Astrophysical Neutrinos	3
2.1.1 Gamma-Ray Bursts Neutrinos	4
2.1.2 Active Galactic Nuclei Neutrinos	4
2.1.3 Neutrino Flux Upper Bound from Cosmic Ray Observations	5
2.2 GZK Neutrinos	6
2.3 Three Types of Neutrino Sources	6
2.4 Neutrino Oscillation Probability Matrix	7
2.5 Neutrino Flavor Ratios	8
3 The Reconstruction of Neutrino Flavor Ratios at Astrophysical Sources	10
3.1 The Reconstruction of Source Flavor Ratios at Energies Lower Than 10^{16} eV	11
3.2 The Reconstruction of Source Flavor Ratios at Energies Higher Than 10^{16} eV	12

4	High Energy Neutrino Spectra and Flux Ratios	16
4.1	Energy Spectra for GRB and GZK Neutrinos	16
4.2	Determining the Flux Ratio of High Energy Neutrinos	21
5	Conclusion	24

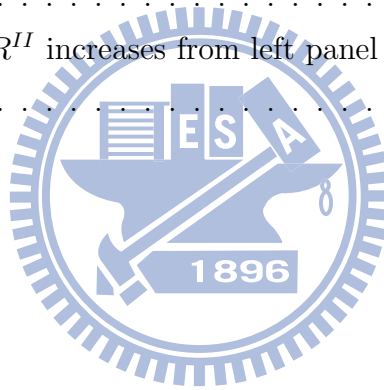


List of Figures

- 3.1 The reconstructed ranges for the neutrino flavor ratios at the source with $\Delta R^I/R^I = 10\%$. The left and right panels are results with the muon-damped source and the pion source as the input true source respectively. The numbers on each side of the triangle denote the flux percentage of a specific flavor of neutrino. The red point marks the muon-damped source $\phi_{0,\mu} = (0, 1, 0)$ and the blue point marks the pion source $\phi_{0,\pi} = (1/3, 2/3, 0)$. Gray and light gray areas respectively denote the 1σ and 3σ ranges for the reconstructed neutrino flavor ratios at the source. 12
- 3.2 The reconstructed ranges for the neutrino flavor ratios at the source with $\Delta R^I/R^I = 10\%$ and $\Delta S/S$ related to the former by the Poisson statistics. The left and right panels are results with the muon-damped source and the pion source as the input true source respectively. Gray and light gray areas in the left (right) panel denote the reconstructed 1σ and 3σ ranges. 13
- 3.3 Reconstructed ranges for muon-damped source with $\Delta R^a/R^a = 10\%$ and $\Delta S^a/S^a = 12\%$. Gray and light gray areas in the left (right) panel denote the reconstructed 1σ and 3σ ranges. The left and right panels correspond to the condition I and II. The pion source can be ruled out at the 3σ level for both conditions. 14

3.4	Reconstructed ranges for muon-damped source with $\Delta R^a/R^a = 10\%$ only. Gray and light gray areas in the left (right) panel denote the reconstructed 1σ and 3σ ranges. The left and right panels correspond to the condition I and II. The pion source can be ruled out at 3σ level for the condition II but not for the condition I even at 1σ level.	14
3.5	Reconstructed ranges for pion source with $\Delta R^a/R^a = 10\%$ and $\Delta S^a/S^a = 12\%$. Gray and light gray areas in the left (right) panel denote the reconstructed 1σ and 3σ ranges. The left and right panels correspond to the condition I and II. The muon-damped source can be ruled out at the 1σ level for both conditions.	15
3.6	Reconstructed ranges for pion source with $\Delta R^a/R^a = 10\%$ only. Gray and light gray areas in the left (right) panel denote the reconstructed 1σ and 3σ ranges. The left and right panels correspond to the condition I and II. For condition I, 3σ limit covers all flavor ratio of source. But the muon-damped source can be ruled out at 1σ level for condition II.	15
4.1	The GZK neutrino spectra. The dashed curve is the prediction for an all-proton primary. The solid lines denote the Fe primary models with the highest and lowest predicted neutrino fluxes [27].	17
4.2	The neutrino fluxes in different flavors, $\epsilon_{\nu_l}^2 \phi_{\nu_l}$ (normalized to $\epsilon_{\nu_e}^2 \phi_{\nu_e}$). ϕ_{ν_l} stands for the combined flux of ν_l and $\bar{\nu}_l$, and these plots are valid for neutrinos produced by any combination of π^+ and π^- decay [2]. The energy scale $\epsilon_{0,\mu}$ is about 4×10^{15} eV in GRB.	18
4.3	Comparison of muon neutrino fluxes (ν_μ and $\bar{\nu}_\mu$ combined) predicted by different models with the upper bound implied by cosmic ray observations [3]. We are interested in the GRB neutrino flux which can be matched with results in Fig. 4.2.	18

4.4	The neutrino flux from GRB source. Blue curve is ν_μ flux in Fig. 4.3. Green curve and red curve represent ν_μ and ν_e fluxes respectively as a result of combining Fig. 4.2 and 4.3.	19
4.5	The comparison of neutrino fluxes from GZK and GRB sources. Green curve represents GRB ν_μ flux, red curve represents GRB ν_e flux. Blue curve represents total GZK neutrino flux with protons as primary ultrahigh energy cosmic rays. Light-blue curve and purple curve are largest and smallest predicted neutrino fluxes with Fe as primary ultrahigh energy cosmic rays.	19
4.6	$\Delta\chi^2 = 1$, $\Delta R^{II}/R^{II}$ increases from left panel to right panel as 5%, 10% and 15%.	23
4.7	$\Delta\chi^2 = 4$, $\Delta R^{II}/R^{II}$ increases from left panel to right panel as 5%, 10% and 15%.	23
4.8	$\Delta\chi^2 = 9$, $\Delta R^{II}/R^{II}$ increases from left panel to right panel as 5%, 10% and 15%.	23



List of Tables

3.1	The definitions of R and S at different energy ranges.	10
4.1	Comparison of integrated GRB and GZK neutrino flux	20
4.2	The ratio of ν_μ flux from GRB to that from GZK	20
4.3	The ratio of ν_μ flux from GRB to that from GZK	20
4.4	The ratio of ν_μ flux from GRB to that from GZK	21
4.5	Neutrino flavor ratio measured on Earth ($E > 10^{16}$ eV)	21



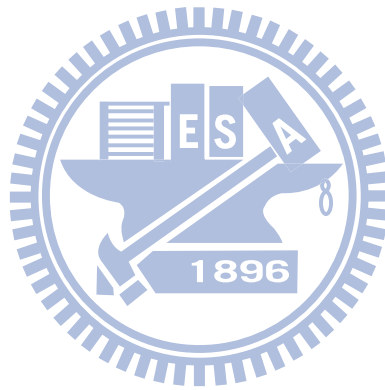
Chapter 1

Introduction

Neutrinos with very high energies ($E \sim 10^{15}$ eV or beyond) come from either the interactions between ultrahigh energy cosmic rays and cosmic microwave background photons, the so called GZK neutrinos [1], or the very high energy tails of astrophysical neutrino spectra. Gamma-ray bursts (GRBs) and active galactic nuclei (AGNs) have been suggested as possible astrophysical sources of high energy neutrinos. Different neutrino sources will induce different neutrino flavor ratios. In this thesis, we are interested in using neutrino flavor ratios as a tool to distinguish GZK neutrino flux from the high energy tails of astrophysical neutrino fluxes. To do this, we propose a statistical method for determining the flavor ratio of very high energy neutrinos and consequently deduce the ratio of GZK neutrino flux to that of astrophysical sources at very high energy.

High energy neutrinos can be generated in astrophysical sources and GZK sources. Neutrino flavor ratio from different sources are different. After the large propagation distance, neutrino flavor composition will change due to neutrino oscillations. The neutrino flavor composition observed on Earth can be determined by the neutrino oscillation probability matrix. Different neutrino sources can be distinguished by measuring the flavor ratios on Earth. The details of these neutrino sources and flavor ratios are presented in Chapter 2. In Chapter 3, we review the statistical method which has been applied to reconstruct neutrino flavor ratio at

the source. In Chapter 4, we first analyze the energy spectrum of GRB neutrinos using formula derived by Kashti and Waxman [2] as well as the result in Ref. [3]. The neutrino flavor ratio at typical GRB source is also calculated with the same formula. Such a flavor ratio is sensitive to neutrino energies. We then compare GRB neutrino flux with that of GZK neutrinos. The ratio between integrated neutrinos fluxes from these two sources are calculated as a function of chosen neutrino threshold energy. Finally we discuss the reconstruction of the above ratio from the measurement of neutrino telescopes. Chapter 5 is the conclusion.



Chapter 2

High Energy Neutrino Sources and Neutrino Flavor Ratio

In this chapter, we introduce the probable high energy neutrino sources. These sources produce high energy neutrinos with three types of flavor ratios. They are referred to as pion source, muon-damped source, and beta-decay source respectively. Due to neutrino oscillations, the neutrino flavor ratio at the astrophysical source could be quite different from that observed on the Earth. Different neutrino sources can be distinguished by measuring the flavor ratio on Earth.

2.1 Astrophysical Neutrinos

High-energy (> 0.1 TeV) neutrino telescopes are under construction to detect cosmologically distant neutrino sources. The motivation for searching cosmological high-energy neutrino sources is based upon the fact that the cosmic-ray energy spectrum extends to $> 10^{20}$ eV and is most likely dominated by an extra-galactic source of protons above $\sim 3 \times 10^{18}$ eV.

The detection can provide the information of fundamental neutrino properties, and also identify the high energy cosmic ray sources. Gamma-ray bursts (GRBs) [4] and active galactic nuclei (AGNs) jets [5] have been suggested as possible sources

of high energy neutrinos.

High energy neutrinos are likely to be associated with the production of high-energy protons and is produced by the decay of charged pions in astrophysical sources,

$$\pi^+ \rightarrow \mu^+ + \nu_\mu \rightarrow e^+ + \nu_e + \bar{\nu}_\mu + \nu_\mu \quad (2.1)$$

$$\pi^- \rightarrow \mu^- + \bar{\nu}_\mu \rightarrow e^- + \nu_e + \nu_\mu + \bar{\nu}_\mu \quad (2.2)$$

These charged pions are produced by photo-meson interaction of the high-energy protons with the radiation field of the source, such as the interaction of protons with photons ($p\gamma$) or nucleons (pp, pn). For neutrinos produced in pp or pn collisions, both π^+ 's and π^- 's are produced. In the case of $p\gamma$ collisions, only π^- 's are produced [2].

2.1.1 Gamma-Ray Bursts Neutrinos

In the GRB fireball model, the observed gamma rays are produced by synchrotron emissions of high-energy electrons accelerated in internal shocks of an expanding relativistic wind. In the region where electrons are accelerated, protons are also expected to be shock accelerated, and their photo-meson interaction with observed burst photons will produce a burst of high-energy neutrinos accompanying the GRB [3, 4].

If GRBs are assumed to be the sources of ultra-high-energy cosmic rays [6, 7], then the GRB neutrino flux is expected to be [3, 4]

$$\begin{aligned} E_\nu^2 \Phi_{\nu_\mu} &\approx E_\nu^2 \Phi_{\bar{\nu}_\mu} \approx E_\nu^2 \Phi_{\nu_e} \\ &\approx 1.5 \times 10^{-9} \left(\frac{f_\pi}{0.2} \right) \min\{1, E_\nu/E_\nu^b\} \text{GeVcm}^{-2}\text{s}^{-1}\text{sr}^{-1}, E_\nu^b \approx 10^{14}\text{eV}. \end{aligned} \quad (2.3)$$

Here, f_π is the fraction of energy lost to pion production by high-energy protons.

2.1.2 Active Galactic Nuclei Neutrinos

AGN have two jets in opposite directions and perpendicular to the accretion disc. The jets accelerate the particles to extremely high energies by Fermi acceleration.

The (Fermi) accelerated ultra high energy protons may collide with other protons or with ambient photons in the vicinity of an AGN or in the associated jets [8]. The interacting chain between high energy protons and gamma rays for generating the pions via Δ^+ resonance is

$$p + \gamma \rightarrow \Delta^+ \rightarrow p + \pi^0 \quad p + \gamma \rightarrow \Delta^+ \rightarrow n + \pi^+ \quad (2.4)$$

Neutrinos are produced by the decay of charged pion as Eq.(2.1). Currently, the photohadronically ($p\gamma$) produced diffuse flux of high energy neutrinos originating from AGNs dominate over the flux from other sources above the relevant atmospheric neutrino background, typically for $E \geq 10^6$ GeV [9, 10].

2.1.3 Neutrino Flux Upper Bound from Cosmic Ray Observations

Cosmic-ray observations above 10^{17} eV indicate that an extra-galactic source of protons dominates the cosmic-ray flux above $\sim 3 \times 10^{18}$ eV, while the flux at lower energies is dominated by heavy ions of galactic origin [11]. From cosmic ray observations, a model-independent upper bound of $E_\nu^2 \Phi_\nu \leq 2 \times 10^{-8} \text{GeV cm}^{-2} \text{s}^{-1} \text{sr}^{-1}$ to the flux of neutrinos produced by $p - \gamma$ interactions for sources optically thin to $p - \gamma$ reactions can be derived [3, 4].

The neutrino flux predictions of AGN jet models are based on two key assumptions. First of all, AGN jets produce the observed gamma-ray background. secondly, high energy photon emission from AGN jets is due to decays of neutral pions produced in photo-meson interactions of protons accelerated in the jet to high energy. Since the neutrino flux predicted by these assumptions is two orders of magnitude higher than the upper bound allowed by cosmic ray observations, at least one of the key assumptions is not valid [3]. The cosmic ray measurements rule out the current version of theories in which the gamma-ray background is due to photo-meson interactions in AGN jets.

Unlike the AGN jet models, the GRB model predicts a neutrino flux satisfying the upper bound from cosmic ray observations [3]. Hence GRB is the more

probable source of high energy neutrinos.

2.2 GZK Neutrinos

Ultrahigh energy protons above the ‘‘GZK cutoff’’ ($> 5 \times 10^{19}$ eV) [12] interact with the cosmic microwave background and infrared background as they propagate over cosmological distances. In this interaction, protons and microwave background photons collide into the resonance state Δ^+ 's, which decay as in Eq. (2.3). Pions decay into neutrinos as the decay chain in Eq.(2.1). The expected spectrum of GZK neutrinos can vary considerably, depending on the precise spectrum and chemical composition injected from the cosmic ray sources.

2.3 Three Types of Neutrino Sources

Most of the astrophysical neutrinos are believed to be produced by the decay of charged pion, which leads to the neutrino flux ratio $\phi_0(\nu_e) : \phi_0(\nu_\mu) : \phi_0(\nu_\tau) = 1 : 2 : 0$ at the astrophysical source where $\phi_0(\nu_\alpha)$ is the sum of ν_α and $\bar{\nu}_\alpha$ flux. This flux ratio results from an implicit assumption that the muon decays into neutrinos before losing a significant fraction of its energy. It is possible that muon quickly loses its energy by interacting with strong magnetic fields or with matter in some sources [13, 14]. Such a muon eventually decays into neutrinos with energies much lower than that of $\nu_\mu(\bar{\nu}_\mu)$ from $\pi^+(\pi^-)$ decays. This type of source is referred to as the muon-damped source, which has a neutrino flavor ratio $\phi_0(\nu_e) : \phi_0(\nu_\mu) : \phi_0(\nu_\tau) = 0 : 1 : 0$. Finally, the third type of source emits neutrons resulting from the photodisassociation of nuclei. As neutrons propagate to the Earth, $\bar{\nu}_e$ are produced from neutron β decays [15], leading to a neutrino flavor ratio $\phi_0(\nu_e) : \phi_0(\nu_\mu) : \phi_0(\nu_\tau) = 1 : 0 : 0$.

We note that there is no flux of ν_τ in the above three sources. Actually, ν_τ may be produced by the production of charmed mesons. However the higher energy threshold and lower cross section for charmed meson production typically imply a

negligible ν_τ fraction.

2.4 Neutrino Oscillation Probability Matrix

Neutrinos are generated or detected with a well defined flavor (electron, muon, tau). It has been demonstrated experimentally that neutrinos are able to oscillate between three flavors while they propagate through space. This quantum mechanical phenomenon was first predicted by Bruno Pontecorvo. Currently, it is understood that oscillations occur due to the fact that the neutrino flavor eigenstates are not identical to the neutrino mass eigenstates (simply called 1, 2, 3). This allows an electron neutrino produced at a given location to be detected as either a muon or tau neutrino with a calculable probability after it has traveled to another location.

In the Standard Model of particle physics, the existence of flavor oscillations implies a nonzero neutrino mass, because the amount of mixing between neutrino flavors depends on the differences in their squared masses.

The neutrino flux at the astrophysical source $\phi_0(\nu_\alpha)$ and that detected on the Earth $\phi(\nu_\alpha)$ is related by

$$\begin{pmatrix} \phi(\nu_e) & \phi(\nu_\mu) & \phi(\nu_\tau) \end{pmatrix} = \begin{pmatrix} \phi_0(\nu_e) & \phi_0(\nu_\mu) & \phi_0(\nu_\tau) \end{pmatrix} \begin{pmatrix} P_{ee} & P_{e\mu} & P_{e\tau} \\ P_{\mu e} & P_{\mu\mu} & P_{\mu\tau} \\ P_{\tau e} & P_{\tau\mu} & P_{\tau\tau} \end{pmatrix}. \quad (2.5)$$

The matrix element $P_{\alpha\beta}$ is the oscillation probability $P(\nu_\alpha \rightarrow \nu_\beta)$. The matrix element $P_{\alpha\beta}$ is given by [16]

$$\begin{aligned} P_{\alpha\beta} = & \delta_{\alpha\beta} - 4 \sum_{i>j} \text{Re}(U_{\alpha i} U_{\beta j}^* U_{\alpha i}^* U_{\beta j}) \sin^2\left(\frac{\Delta m_{ij}^2 L}{4E}\right) + \\ & 4 \sum_{i>j} \text{Im}(U_{\alpha i} U_{\beta j}^* U_{\alpha i}^* U_{\beta j}) \sin\left(\frac{\Delta m_{ij}^2 L}{4E}\right) \cos\left(\frac{\Delta m_{ij}^2 L}{4E}\right). \end{aligned} \quad (2.6)$$

Here, $\Delta m_{ij}^2 \equiv m_i^2 - m_j^2$ is in eV^2 , L is in km, and E is in GeV. By using the

factors of \hbar and c , one has

$$\Delta m_{ij}^2(L/4E) \simeq 1.27 \Delta m_{ij}^2(\text{eV}^2) \frac{L(\text{km})}{E(\text{GeV})}. \quad (2.7)$$

U is the Pontecorvo-Maki-Nagakawa-Sakata mixing matrix

$$U = \begin{pmatrix} c_{12}c_{13} & s_{12}c_{13} & s_{13}e^{-i\delta} \\ -s_{12}c_{23} - c_{12}s_{23}s_{13}e^{i\delta} & c_{12}c_{23} - s_{12}s_{23}s_{13}e^{i\delta} & s_{23}c_{13} \\ s_{12}s_{23} - c_{12}c_{23}s_{13}e^{i\delta} & -c_{12}s_{23} - s_{12}c_{23}s_{13}e^{i\delta} & c_{23}c_{13} \end{pmatrix}, \quad (2.8)$$

where $c_{ij} = \cos\theta_{ij}$, $s_{ij} = \sin\theta_{ij}$, and δ is the CP violating phase.

Despite the oscillation, the total neutrino number is conserved such that $\sum_{\beta} P_{\alpha\beta} = 1$. However, in the presence of a non negligible decay probability or of transitions to additional sterile states, the above sum can be less than unity. In most cases, the neutrino oscillation length $\lambda_{ij} = 4\pi E / |\Delta m_{ij}^2|$ is negligibly short compared to the typical astrophysical distance. Hence for astrophysical neutrinos, it is a good approximation to consider only the averaged oscillation probability which takes the form [17, 18]:

$$P(\nu_{\alpha} \rightarrow \nu_{\beta}) = \sum_i |U_{\alpha i}|^2 |U_{\beta i}|^2 \quad (2.9)$$

The current best-fit values as well as the allowed 1σ and 3σ range of the mixing angles are [19]

$$\sin^2 \theta_{12} = 0.32_{-0.02,0.06}^{+0.02,0.08}, \sin^2 \theta_{23} = 0.45_{-0.06,0.13}^{+0.09,0.19}, \sin^2 \theta_{13} < 0.019(0.050) \quad (2.10)$$

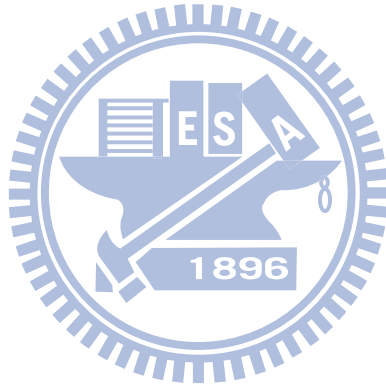
2.5 Neutrino Flavor Ratios

The capability of distinguishing between different neutrino sources depends on the knowledge of neutrino mixing parameters and the achievable accuracies in measuring the neutrino flavor ratios $R \equiv \phi(\nu_{\mu})/(\phi(\nu_e) + \phi(\nu_{\tau}))$ [20] and $S \equiv \phi(\nu_e)/\phi(\nu_{\tau})$ [21] on Earth. R is used to distinguish shower-like events from track-like ones, while S is used to distinguish between shower-like events.

The flux ratio of the pion source is $\phi_0(\nu_e) : \phi_0(\nu_{\mu}) : \phi_0(\nu_{\tau}) = 1 : 2 : 0$ at the source, while the flux ratio observed on Earth is $\phi(\nu_e) : \phi(\nu_{\mu}) : \phi(\nu_{\tau}) = 1 : 1 : 1$.

Muon-damped source is $\phi_0(\nu_e) : \phi_0(\nu_\mu) : \phi_0(\nu_\tau) = 0 : 1 : 0$ at the source, and the flux ratio observed on Earth is $\phi(\nu_e) : \phi(\nu_\mu) : \phi(\nu_\tau) = 1.8 : 1.8 : 1$. Hence we have $R = 0.5$ and $S = 1$ for the pion source, while $R = 0.64$ and $S = 0.56$ for the muon-damped source.

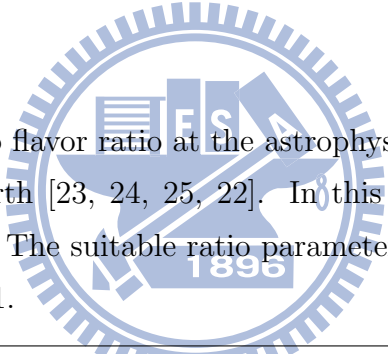
The ratio parameters R and S are suitable for $E_\nu < 10^{16}$ eV. At energies higher than 10^{16} eV, $R \equiv e/(\mu + \tau)$ and $S \equiv \mu/t$ is a more suitable set of parameters since tau is a track-like event at high energies [22].



Chapter 3

The Reconstruction of Neutrino Flavor Ratios at Astrophysical Sources

One can infer the neutrino flavor ratio at the astrophysical source from the flavor ratio we measured on Earth [23, 24, 25, 22]. In this chapter we review results obtained in Refs. [23, 22]. The suitable ratio parameters for flavor reconstruction is summarized in Table 3.1.



Condition I : $E_\nu < 33$ PeV	Condition II : $E_\nu > 33$ PeV
$R^I \equiv \phi(\nu_\mu)/(\phi(\nu_e) + \phi(\nu_\tau))$	$R^{II} \equiv \phi(\nu_e)/(\phi(\nu_\mu) + \phi(\nu_\tau))$
$S^I \equiv \phi(\nu_e)/\phi(\nu_\tau)$	$S^{II} \equiv \phi(\nu_\mu)/\phi(\nu_\tau)$

Table 3.1: The definitions of R and S at different energy ranges.

3.1 The Reconstruction of Source Flavor Ratios at Energies Lower Than 10^{16} eV

To do the reconstruction with a statistical analysis, we use the following best-fit values and 1σ ranges of neutrino mixing parameters set1 $\sin^2 \theta_{12} = 0.32_{-0.02}^{+0.02}$, $\sin^2 \theta_{23} = 0.45_{-0.06}^{+0.09}$, $\sin^2 \theta_{13} < 0.019$ in Ref. [19].

The fitting to the neutrino flavor ratios at the source is facilitated through

$$\chi^2 = \left(\frac{R_{th}^I - R_{exp}^I}{\sigma_{R_{exp}^I}}\right)^2 + \left(\frac{S_{th}^I - S_{exp}^I}{\sigma_{S_{exp}^I}}\right)^2 + \sum_{jk=12,23,13} \left(\frac{S_{jk}^2 - (S_{jk}^2)_{best\,fit}}{\sigma_{S_{jk}^2}}\right)^2, \quad (3.1)$$

with $\sigma_{R_{exp}^I} = (\Delta R^I/R^I)R_{exp}^I$, $\sigma_{S_{exp}^I} = (\Delta S^I/S^I)S_{exp}^I$, $S_{jk}^2 \equiv \sin^2 \theta_{jk}$ and $\sigma_{S_{jk}^2}$ the 1σ range for S_{jk}^2 . Here R_{th}^I and S_{th}^I are theoretical predicted values for R^I and S^I respectively while R_{exp}^I and S_{exp}^I are experimentally measured values. In our analysis, we scan all possible neutrino flavor ratios at the source that give rise to a specific χ^2 value. Since we have taken R_{exp}^I and S_{exp}^I as those generated by input true values of initial neutrino flavor ratios and neutrino mixing parameters, we have $(\chi^2)_{min} = 0$ occurring at these input true values of parameters. Hence the boundaries for 1σ and 3σ ranges of initial neutrino flavor ratios are given by $\Delta\chi^2 = 2.3$ and $\Delta\chi^2 = 11.8$ respectively where $\Delta\chi^2 \equiv \chi^2 - (\chi^2)_{min} = \chi^2$ in our analysis [23].

By measuring R alone from either an input pion source or an input muon-damped source with a precision $\Delta R^I/R^I = 10\%$, the reconstructed 3σ range for the initial neutrino flavor ratio is as large as the entire physical range as shown in Fig. 3.1. By measuring both R and S from an input muon-damped source, we can see from Fig. 3.2 that the pion source can be ruled out at the 3σ level for the parameter sets 1 and 2 with $\Delta R^I/R^I = 10\%$ and $\Delta S^I/S^I$ related to the former by the Poisson statistics.

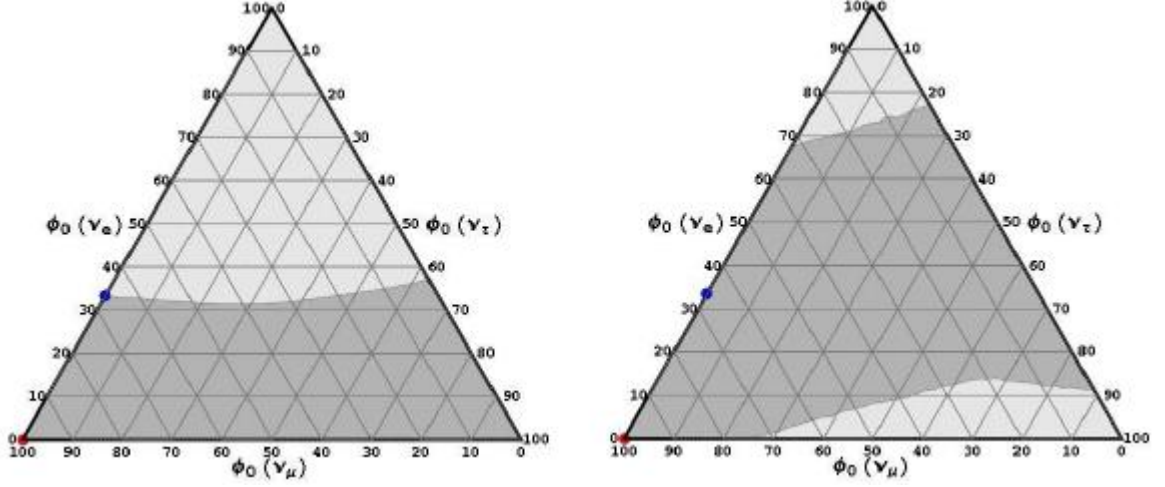


Figure 3.1: The reconstructed ranges for the neutrino flavor ratios at the source with $\Delta R^I/R^I = 10\%$. The left and right panels are results with the muon-damped source and the pion source as the input true source respectively. The numbers on each side of the triangle denote the flux percentage of a specific flavor of neutrino. The red point marks the muon-damped source $\phi_{0,\mu} = (0, 1, 0)$ and the blue point marks the pion source $\phi_{0,\pi} = (1/3, 2/3, 0)$. Gray and light gray areas respectively denote the 1σ and 3σ ranges for the reconstructed neutrino flavor ratios at the source.

3.2 The Reconstruction of Source Flavor Ratios at Energies Higher Than 10^{16} eV

Let us take the muon-damped source as the input true source and consider its reconstruction. The reconstructed regions of neutrino flavor ratio are comparable for $a = \text{I}$ and II . For an input muon-damped source, the pion source can be ruled out at the 3σ level as shown in Fig. 3.3.

It is well known that measuring R^a is easier than measuring S^a for neutrino telescopes. If the measurements on S^a are not available, the results for flavor-ratio reconstruction are quite different. Fig. 3.4 shows the reconstructed flavor ratios with $\Delta R^a/R^a = 10\%$. The reconstructed region of neutrino flavor ratio for $a = \text{I}$

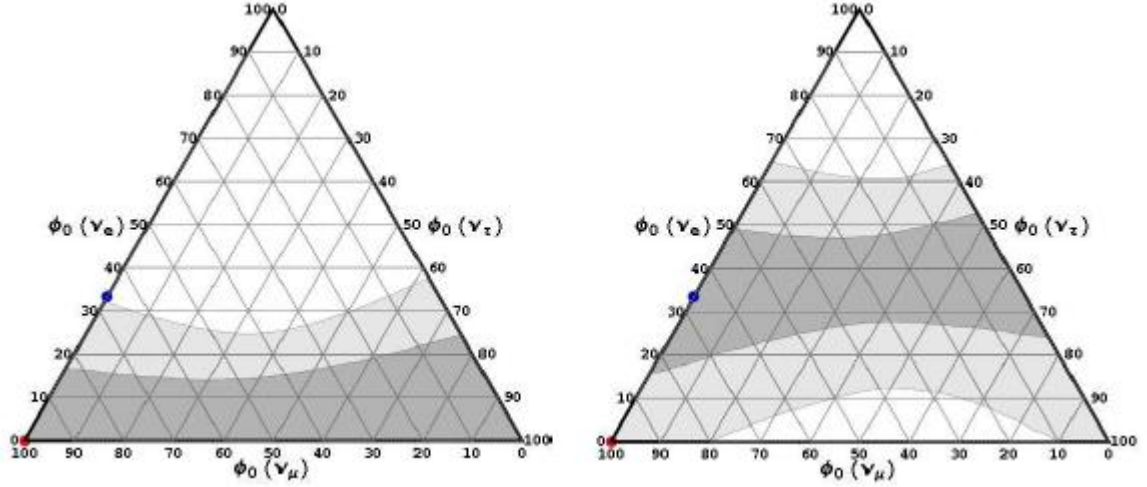


Figure 3.2: The reconstructed ranges for the neutrino flavor ratios at the source with $\Delta R^I/R^I = 10\%$ and $\Delta S/S$ related to the former by the Poisson statistics. The left and right panels are results with the muon-damped source and the pion source as the input true source respectively. Gray and light gray areas in the left (right) panel denote the reconstructed 1σ and 3σ ranges.

is much larger than that for a =II. The pion source can only be ruled out at 3σ level for the condition II but not for the condition I.

For an input pion source, the muon-damped source can be ruled out at the 1σ level as shown in Fig. 3.5 for both energy conditions. If one only measures R^a with $\Delta R^a/R^a = 10\%$, it is shown in Fig. 3.6 that the reconstructed region for a =I covers all physical parameter space while the reconstructed region for a =II remains comparable to that in Fig. 3.5. Once again, the muon-damped source can be ruled out for condition II at 1σ level, but not for condition I at the same confidence level. From the reconstructions of pion source and muon-damped source, it is evident that this new parameter R^{II} is more efficient than R^I for reducing the source uncertainty if the measurements on S^a are not available.

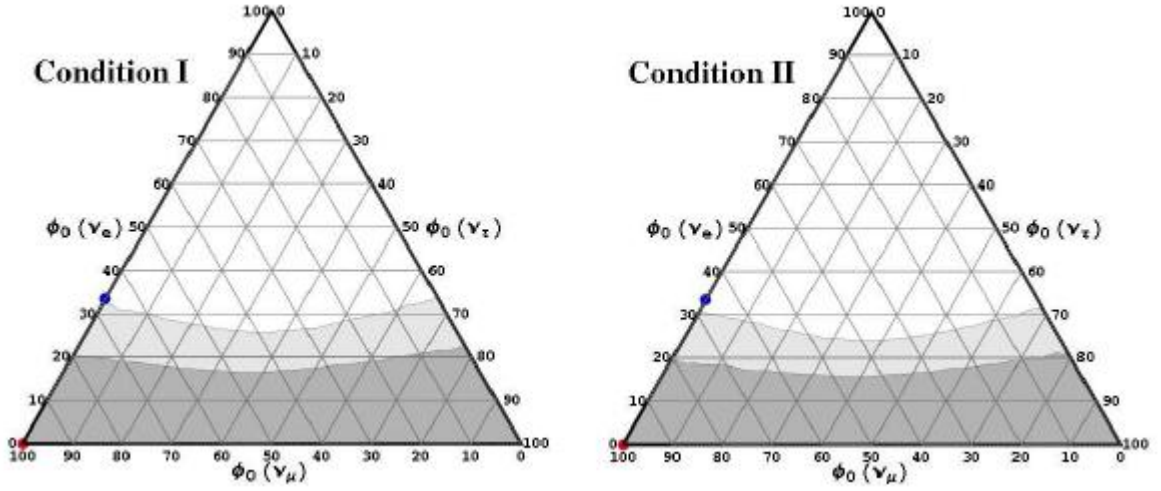


Figure 3.3: Reconstructed ranges for muon-damped source with $\Delta R^a/R^a = 10\%$ and $\Delta S^a/S^a = 12\%$. Gray and light gray areas in the left (right) panel denote the reconstructed 1σ and 3σ ranges. The left and right panels correspond to the condition I and II. The pion source can be ruled out at the 3σ level for both conditions.

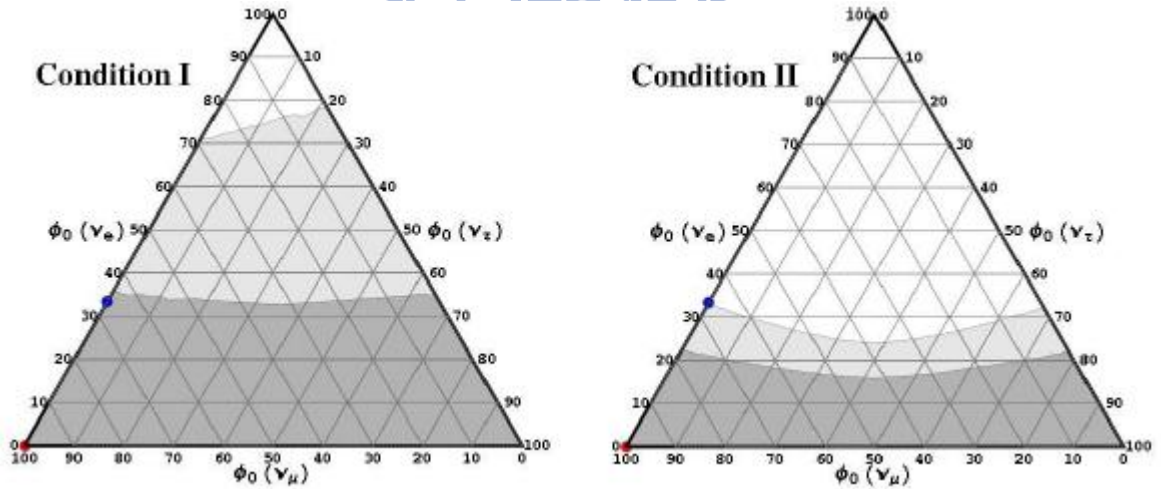


Figure 3.4: Reconstructed ranges for muon-damped source with $\Delta R^a/R^a = 10\%$ only. Gray and light gray areas in the left (right) panel denote the reconstructed 1σ and 3σ ranges. The left and right panels correspond to the condition I and II. The pion source can be ruled out at 3σ level for the condition II but not for the condition I even at 1σ level.

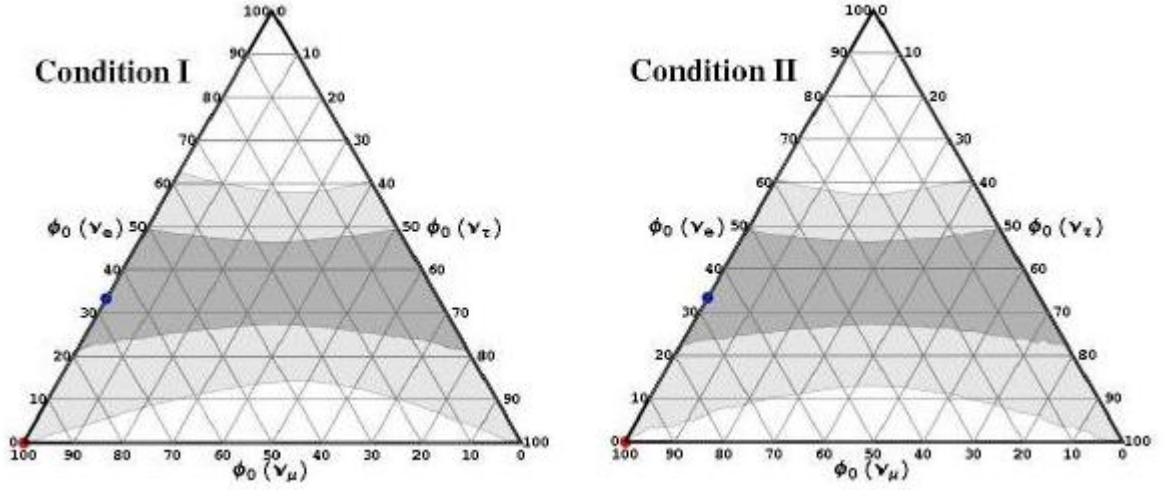


Figure 3.5: Reconstructed ranges for pion source with $\Delta R^a/R^a = 10\%$ and $\Delta S^a/S^a = 12\%$. Gray and light gray areas in the left (right) panel denote the reconstructed 1σ and 3σ ranges. The left and right panels correspond to the condition I and II. The muon-damped source can be ruled out at the 1σ level for both conditions.

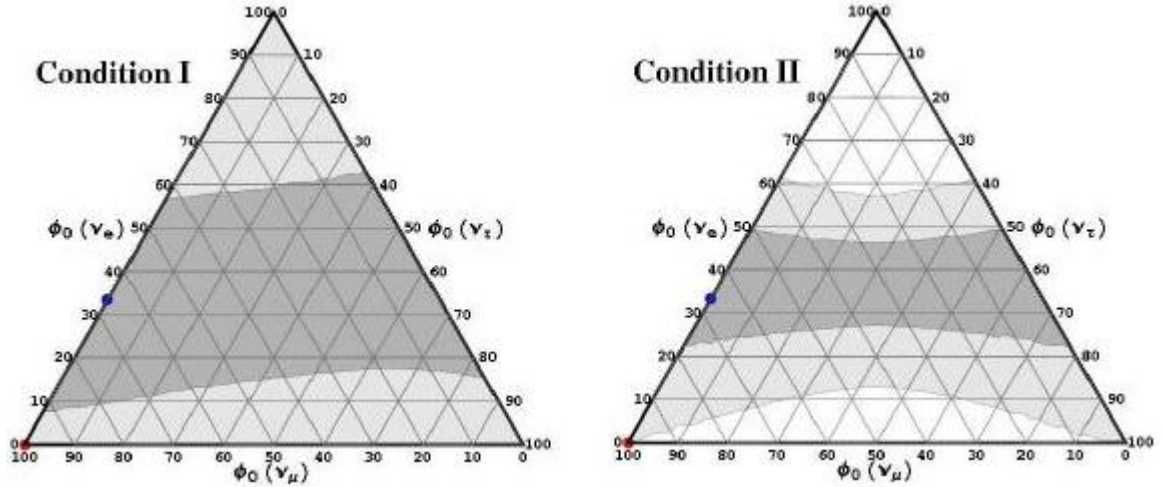


Figure 3.6: Reconstructed ranges for pion source with $\Delta R^a/R^a = 10\%$ only. Gray and light gray areas in the left (right) panel denote the reconstructed 1σ and 3σ ranges. The left and right panels correspond to the condition I and II. For condition I, 3σ limit covers all flavor ratio of source. But the muon-damped source can be ruled out at 1σ level for condition II.

Chapter 4

High Energy Neutrino Spectra and Flux Ratios

High energy neutrinos can be generated by astrophysical sources and GZK interactions. These sources of neutrinos have distinct flavor ratios. For astrophysical sources, the neutrino flavor ratios depend on energies [2, 26]. In this chapter, we propose a statistical method for determining the flux ratio of the above two sources of very high energy neutrinos.

4.1 Energy Spectra for GRB and GZK Neutrinos

In this section, we compare the GZK neutrino spectra (Fig. 4.1) [27] with the astrophysical neutrino spectra (Figs. 4.2,4.3) [2] for determining the relative contributions of these sources to the total high-energy neutrino flux.

We note that Fig. 4.2 gives the energy dependencies of GRB ν_e and ν_μ fluxes while Fig. 4.3 gives the normalization of GRB ν_μ flux at 10^{14} eV. Combining both figures, we obtain GRB neutrino flux as presented in Fig. 4.4. The blue curve is the flux in Fig. 4.3, red curve and green curve are ν_e and ν_μ fluxes respectively. The neutrino spectrum is steep at high energy ($> 10^{16}$ eV), where

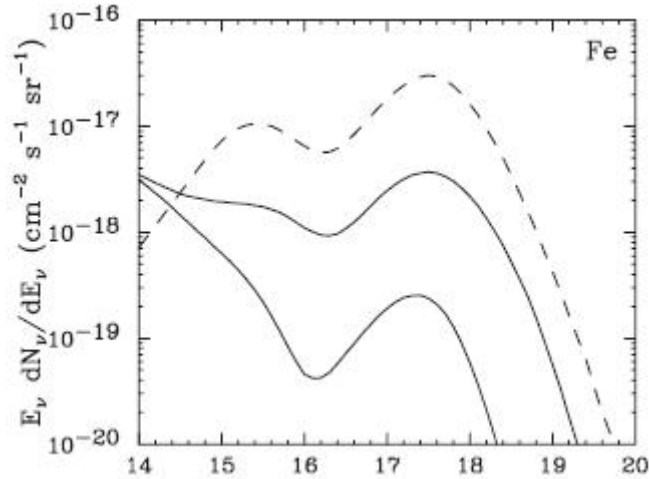


Figure 4.1: The GZK neutrino spectra. The dashed curve is the prediction for an all-proton primary. The solid lines denote the Fe primary models with the highest and lowest predicted neutrino fluxes [27].

neutrinos are produced by the decay of muons and pions whose lifetime $\tau_{\mu,\pi}$ exceeds the characteristic time for energy loss due to adiabatic expansion and synchrotron emission.

GRB and GZK neutrino spectra are compared in Fig. 4.5. We calculate the integrated neutrino flux with threshold energy varied from 10^{14} eV to 10^{18} eV. The results are shown in Table 4.1. We calculate the ratio of GRB muon neutrino flux to GZK muon neutrino flux as shown in Table 4.2. GRB neutrino sources dominate when threshold energy is below 10^{16} eV, while GZK neutrino sources dominate as threshold energy is higher than 10^{17} eV. For a 10^{16} eV threshold energy, the contribution of GRB and GZK to the total flux is almost the same. In Table 4.3 (Table 4.4), we calculate the muon-neutrino flux ratio of GRB source to GZK source with Fe as primary ultrahigh energy cosmic rays. GZK neutrino source dominates as the neutrino energy is higher than 10^{17} eV (Table 4.3) and 10^{18} eV (Table 4.4).

If we take the ratio of total neutrino flux from muon-damped source to that from pion source as $c/(1-c)$, the neutrino flux ratio r of GRB to GZK in Table

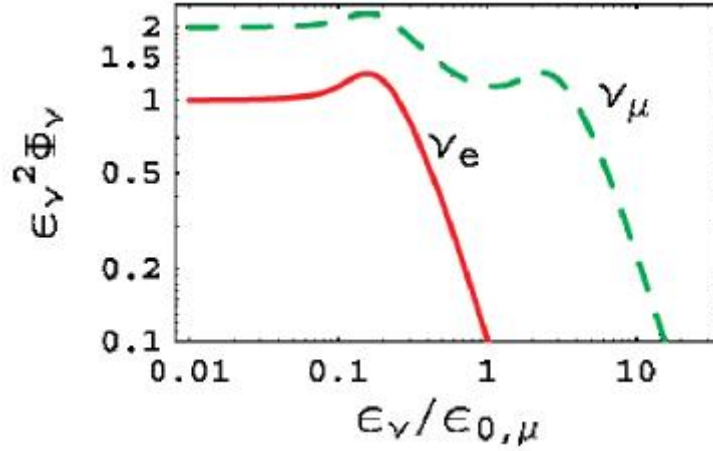


Figure 4.2: The neutrino fluxes in different flavors, $\epsilon_{\nu_l}^2 \phi_{\nu_l}$ (normalized to $\epsilon_{\nu_e}^2 \phi_{\nu_e}$). ϕ_{ν_l} stands for the combined flux of ν_l and $\bar{\nu}_l$, and these plots are valid for neutrinos produced by any combination of π^+ and π^- decay [2]. The energy scale $\epsilon_{0,\mu}$ is about 4×10^{15} eV in GRB.

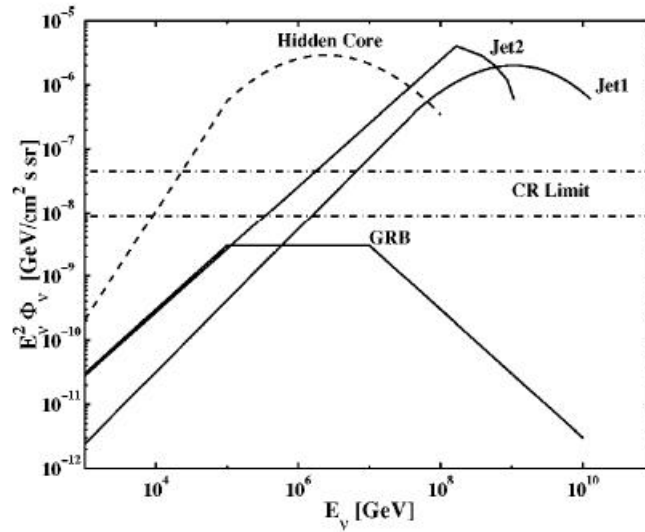


Figure 4.3: Comparison of muon neutrino fluxes (ν_μ and $\bar{\nu}_\mu$ combined) predicted by different models with the upper bound implied by cosmic ray observations [3]. We are interested in the GRB neutrino flux which can be matched with results in Fig. 4.2.

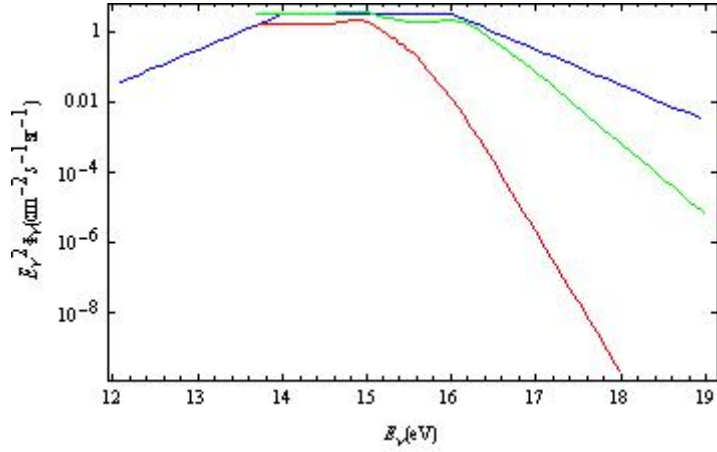


Figure 4.4: The neutrino flux from GRB source. Blue curve is ν_μ flux in Fig. 4.3. Green curve and red curve represent ν_μ and ν_e fluxes respectively as a result of combining Fig. 4.2 and 4.3.

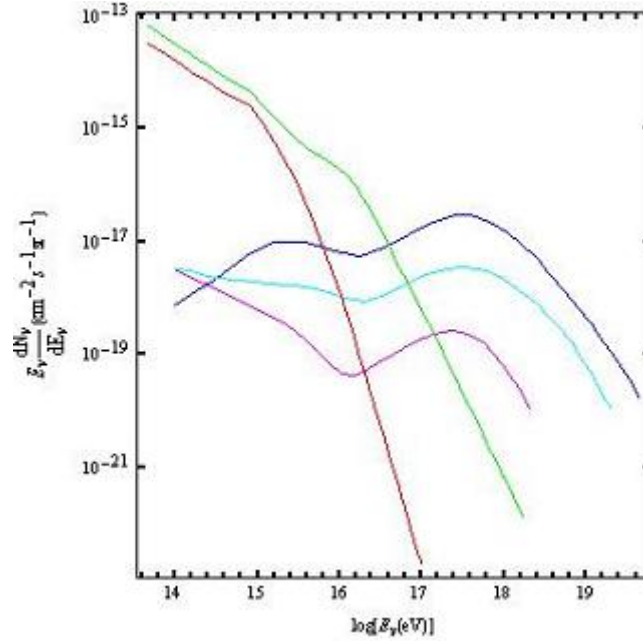


Figure 4.5: The comparison of neutrino fluxes from GZK and GRB sources. Green curve represents GRB ν_μ flux, red curve represents GRB ν_e flux. Blue curve represents total GZK neutrino flux with protons as primary ultrahigh energy cosmic rays. Light-blue curve and purple curve are largest and smallest predicted neutrino fluxes with Fe as primary ultrahigh energy cosmic rays.

log[E(eV)]	N(cm ⁻² s ⁻¹ sr ⁻¹)				
	GRB ν_e	GRB ν_μ	GZK proton	GZK Fe-max	GZK Fe-min
> 14	3.60×10^{-14}	6.76×10^{-14}	1.17×10^{-16}	2.13×10^{-17}	4.76×10^{-18}
> 15	4.84×10^{-16}	1.78×10^{-15}	1.06×10^{-16}	1.51×10^{-17}	1.14×10^{-18}
> 16	2.58×10^{-19}	7.72×10^{-17}	8.57×10^{-17}	1.17×10^{-17}	6.53×10^{-19}
> 17	4.14×10^{-24}	2.20×10^{-19}	6.52×10^{-17}	8.59×10^{-18}	3.84×10^{-19}
> 18		2.29×10^{-22}	1.02×10^{-17}	1.72×10^{-18}	1.29×10^{-20}

Table 4.1: Comparison of integrated GRB and GZK neutrino flux

log[E(eV)]	N(cm ⁻² s ⁻¹ sr ⁻¹)		Flux Ratio
	GRB ν_μ	GZK ν_μ (proton)	$r=\text{GRB}/\text{GZK}$
> 14	6.76×10^{-14}	0.78×10^{-16}	870
> 15	1.78×10^{-15}	0.71×10^{-16}	25
> 16	7.72×10^{-17}	5.71×10^{-17}	1.4
> 17	2.20×10^{-19}	4.35×10^{-17}	5.1×10^{-3}
> 18	2.29×10^{-22}	0.68×10^{-17}	3.4×10^{-5}

Table 4.2: The ratio of ν_μ flux from GRB to that from GZK

log[E(eV)]	N(cm ⁻² s ⁻¹ sr ⁻¹)		Flux Ratio
	GRB ν_μ	GZK ν_μ (Fe-max)	$r=\text{GRB}/\text{GZK}$
> 14	6.8×10^{-14}	1.4×10^{-17}	4.8×10^4
> 15	1.8×10^{-15}	1.0×10^{-17}	176
> 16	7.7×10^{-17}	0.8×10^{-17}	9.9
> 17	2.2×10^{-19}	5.7×10^{-18}	0.04
> 18	2.3×10^{-22}	1.2×10^{-18}	2.0×10^{-4}

Table 4.3: The ratio of ν_μ flux from GRB to that from GZK

4.2-4.4 is equal to $3c/2(1 - c)$. For example, the neutrino flux ratio of GRB to GZK proton is $r \equiv 3c/2(1 - c) = 1.4$ when the threshold energy is 10^{16} eV. Hence the fraction of contribution of GRB neutrino source to the total neutrino flux is $c=0.5$. We also determine the neutrino flavor ratio measured on Earth in Table 4.5. With these neutrino flavor ratios, we can distinguish different sources.

log[E(eV)]	N(cm ⁻² s ⁻¹ sr ⁻¹)		Flux Ratio
	GRB ν_μ	GZK ν_μ (Fe-min)	$r=\text{GRB}/\text{GZK}$
> 14	6.8×10^{-14}	3.2×10^{-18}	2.1×10^4
> 15	1.8×10^{-15}	0.8×10^{-18}	2.3×10^3
> 16	7.7×10^{-17}	4.4×10^{-19}	177
> 17	2.2×10^{-19}	2.6×10^{-19}	0.9
> 18	2.3×10^{-22}	0.9×10^{-20}	0.03

Table 4.4: The ratio of ν_μ flux from GRB to that from GZK

Sources	c	$\phi_{0,c} = ((1 - c)/3, (2 + c)/3, 0)$	$\phi_c = P\phi_{0,c}$	R^{II}
GRB+GZK proton	0.47	(0.18, 0.82, 0)	(0.26, 0.38, 0.36)	0.35
GRB+GZK Fe-max	0.86	(0.05, 0.95, 0)	(0.21, 0.41, 0.38)	0.27
GRB+GZK Fe-min	0.99	(0.003, 0.997, 0)	(0.19, 0.42, 0.39)	0.24

Table 4.5: Neutrino flavor ratio measured on Earth ($E > 10^{16}$ eV)

4.2 Determining the Flux Ratio of High Energy Neutrinos

We determine the flux ratio of very high energy neutrinos which come from GRB and GZK sources. The former is a muon-damped source with $\phi_0(\nu_e) : \phi_0(\nu_\mu) : \phi_0(\nu_\tau) = 0 : 1 : 0$ and the latter is a pion source with $\phi_0(\nu_e) : \phi_0(\nu_\mu) : \phi_0(\nu_\tau) = 1/3 : 2/3 : 0$. Assuming the ratio of muon-damped source to pion source is $c/(1 - c)$, the

neutrino flavor ratio is then $\phi_0(\nu_e) : \phi_0(\nu_\mu) : \phi_0(\nu_\tau) = (1-c)/3 : (2+c)/3 : 0$. Due to the neutrino oscillation (Eq. 4.1), the fluxes $\phi(\nu_e)$, $\phi(\nu_\mu)$ and $\phi(\nu_\tau)$ measured on the Earth are different from those at the source. They are given by

$$\begin{pmatrix} \phi(\nu_e) & \phi(\nu_\mu) & \phi(\nu_\tau) \end{pmatrix} = \begin{pmatrix} (1-c)/3 & (2+c)/3 & 0 \end{pmatrix} \begin{pmatrix} P_{ee} & P_{e\mu} & P_{e\tau} \\ P_{\mu e} & P_{\mu\mu} & P_{\mu\tau} \\ P_{\tau e} & P_{\tau\mu} & P_{\tau\tau} \end{pmatrix} \quad (4.1)$$

We use the statistical method mentioned in Chapter 3 to reconstruct the neutrino flavor ratio at the source. In this high energy limit, one measures $R^{II} = e/\mu + \tau$. Hence

$$\chi^2 = \left(\frac{R^{II}_{th} - R^{II}_{exp}}{\sigma_{R^{II}_{exp}}} \right)^2 + \sum_{jk=12,23,13} \left(\frac{S_{jk}^2 - (S_{jk})_{bestfit}^2}{\sigma_{S_{jk}^2}} \right)^2. \quad (4.2)$$

We determine whether the reconstructed ratio c_{output} is consistent with the input ratio c_{input} . In χ^2 fitting, we also take $\Delta R^{II}/R^{II}$ as 5%, 10% and 15% respectively. The probable ranges of the flux ratio “ c ” are presented in Fig. 4.6-4.8. The color regions in Fig. 4.6, 4.7 and 4.8 correspond to 1σ , 2σ and 3σ reconstructed ranges for the ratio c . We find that the reconstructed ratio c_{output} is better constrained when the input ratio c_{input} is larger. A larger value of c_{input} implies the dominance of GRB neutrino source. In this situation, we can clearly reconstruct the very high energy neutrino source. However, for a small c_{input} (GZK dominant case), one can not rule out the GRB source in the flavor reconstruction since the allowed range for c_{output} is large.

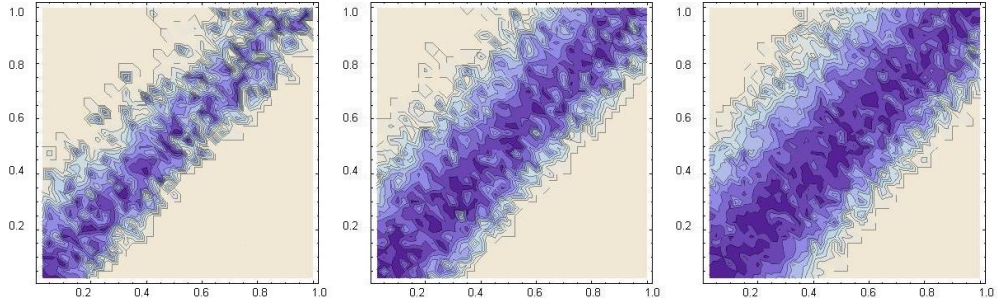


Figure 4.6: $\Delta\chi^2 = 1$, $\Delta R^{II}/R^{II}$ increases from left panel to right panel as 5%, 10% and 15%.

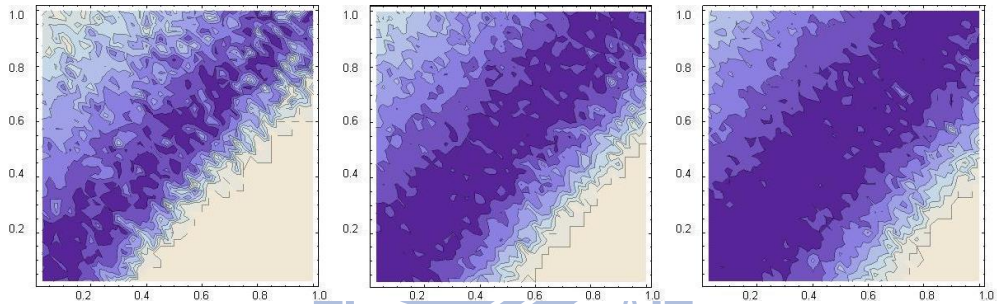


Figure 4.7: $\Delta\chi^2 = 4$, $\Delta R^{II}/R^{II}$ increases from left panel to right panel as 5%, 10% and 15%.

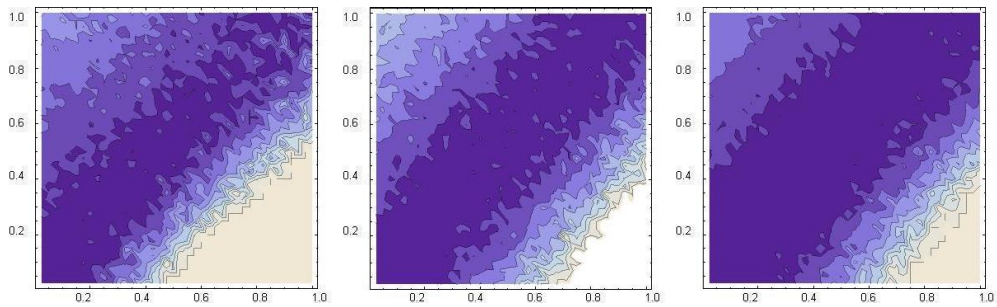


Figure 4.8: $\Delta\chi^2 = 9$, $\Delta R^{II}/R^{II}$ increases from left panel to right panel as 5%, 10% and 15%.

Chapter 5

Conclusion

Flavor ratio of astrophysical neutrinos varies with the neutrino energy and the neutrino spectra. It has been argued in Ref. [2, 27] that this ratio evolves from that of a pion source to that of a muon-damped source as neutrino energy increases. However, the flavor ratio of the GZK neutrino is fixed to be that of a pion source.

The source composition of high energy neutrinos in different energy range has been calculated in Table 4.2. The contribution of integrated GRB and GZK (proton dominant) neutrino fluxes to the total integrated flux is almost the same for 10^{16} eV threshold energy. GRB neutrino source dominates when the threshold energy is below 10^{16} eV, while GZK neutrino source dominates as the energy threshold is above 10^{17} eV.

We have presented the results for the reconstruction of source composition of very high energy neutrino flux. The reconstructed composition c_{output} is better constrained when the input composition c_{input} is larger. A larger value of c_{input} means that GRB neutrino source dominates. In contrast, c_{output} is poorly constrained for a small c_{input} .

In summary, the flavor ratio of astrophysical neutrinos in different energy range is worth studying. We can infer the composition of neutrino sources from such a study.

Bibliography

- [1] V.S. Berezinsky and G.T. Zatsepin, Phys. Lett. 28B, 423 (1969). For a recent discussion, see R. Engel, D. Seckel, and T. Stanev, Phys. Rev. D 64, 093010 (2001).
- [2] T. Kashti and E. Waxman, Phys. Rev. Lett. 95, 181101 (2005).
- [3] E. Waxman and J. N. Bahcall, Phys. Rev. D 59, 023002 (1998).
- [4] E. Waxman and J. N. Bahcall, Phys. Rev. Lett. 78, 2292 (1997).
- [5] K. Mannheim, Astropart. Phys. 3, 295 (1995); F. Halzen and E. Zas, Astrophys. J. 488, 669 (1997); R. J. Protheroe, Adelaide Report No. ADP-AT-96-7, astro-ph/9607165.
- [6] E. Waxman, Phys. Rev. Lett. 75, 386 (1995).
- [7] M. Milgrom and V. Usov, Astrophys. J. 449, L37 (1995); M. Vietri, ibid. 453, 883 (1995).
- [8] For a review, see, for example, H. Athar, Chinese Journal of Physics Vol. 42 , No. 1.
- [9] F. Halzen, Lectures on neutrino astronomy: Theory and experiment, lectures given at Theoretical Advanced Study Institute in Elementary Particle Physics (TASI 98), Boulder, USA, arXiv:astro-ph/9810368.

- [10] R. J. Protheroe, High energy neutrino astrophysics, invited talk given at 18th International Conference on Neutrino Physics and Astrophysics (Neutrino 98), Takayama, Japan, Nucl. Phys. Proc. Suppl. 77, 465 (1999) [arXiv:astro-ph/9809144].
- [11] A. A. Watson, Nucl. Phys. B (Proc. Suppl.) 22B, 116 (1991); D. J. Bird et al., Phys. Rev. Lett. 71, 3401 (1993); S. Yoshida et al., Astropart. Phys. 3, 151 (1995).
- [12] K. Greisen, Phys. Rev. Lett. 16, 748 (1966); G. T. Zatsepin and V. A. Kuzmin, Pis'ma Zh. Eksp. Teor. Fiz. 4, 114 (1966) [JETP Lett. 4, 78 (1966)].
- [13] J. P. Rachen and P. Meszaros, Phys. Rev. D 58, 123005 (1998).
- [14] M. Kachelriess, S. Ostapchenko and R. Tomas, Phys. Rev. D 77, 023007 (2008).
- [15] L. A. Anchordoqui, H. Goldberg, F. Halzen and T. J. Weiler, Phys. Lett. B 593, 42 (2004).
- [16] E. Eichten and K. Lane, Phys. Lett. 90B, 125 (1980).
- [17] J. G. Learned and S. Pakvasa, Astropart. Phys. 3, 267 (1995).
- [18] H. Athar, M. Jezabek and O. Yasuda, Phys. Rev. D 62, 103007 (2000); L. Bento, P. Keranen and J. Maalampi, Phys. Lett. B 476, 205 (2000).
- [19] M. C. Gonzalez-Garcia and M. Maltoni, Phys. Rep. 460, 1 (2008), and references therein.
- [20] P. D. Serpico and M. Kachelrieß, Phys. Rev. Lett. 94, 211102 (2005).
- [21] W. Winter, Phys. Rev. D 74, 033015 (2006).
- [22] T. C. Liu, M. A. Huang and G. L. Lin, arXiv:1004.5154 [hep-ph].

- [23] K. C. Lai, G. L. Lin, and T. C. Liu, Phys. Rev. D 80, 103005 (2009).
- [24] A. Esmaili and Y. Farzan, Nucl. Phys. B 821, 197 (2009).
- [25] S. Choubey and W. Rodejohann, Phys. Rev. D 80, 113006 (2009).
- [26] P. Lipari, M. Lusignoli and D. Meloni, Phys. Rev. D **75**, 123005 (2007) [arXiv:0704.0718 [astro-ph]].
- [27] Luis A. Anchordoqui, Haim Goldberg, Dan Hooper, Subir Sarkar, and Andrew Taylor, Phys. Rev. D 76, 123008 (2007).

